Jyväskylän yliopiston julkaisuarkisto
Jyväskylä University Digital Archive

UNIVERSITY OF JYVÄSKYLÄ

This is an electronic reprint of the original article.
This reprint *may differ* from the original in pagination and typographic detail.

Author(s): PHENIX Collaboration

Title: Measurement of the higher-order anisotropic flow coefficients for identified hadrons in Au + Au collisions at √sNN = 200 GeV

Year: 2016

Version:

Please cite the original version:

PHENIX Collaboration. (2016). Measurement of the higher-order anisotropic flow coefficients for identified hadrons in Au + Au collisions at √sNN = 200 GeV. Physical Review C, 93(5), Article 051902(R). https://doi.org/10.1103/PhysRevC.93.051902

All material supplied via JYX is protected by copyright and other intellectual property rights, and duplication or sale of all or part of any of the repository collections is not permitted, except that material may be duplicated by you for your research use or educational purposes in electronic or print form. You must obtain permission for any other use. Electronic or print copies may not be offered, whether for sale or otherwise to anyone who is not an authorised user.

PHYSICAL REVIEW C **93**, 051902(R) (2016)

Measurement of the higher-order anisotropic flow coefficients for identified hadrons in Au + Au collisions at $\sqrt{s_{NN}} = 200$ GeV

A. Adare,[13] S. Afanasiev,[30] C. Aidala,[43,44] N. N. Ajitanand,[64] Y. Akiba,[58,59] H. Al-Bataineh,[52] J. Alexander,[64] K. Aoki,[35,58] Y. Aramaki,[12] E. T. Atomssa,[36] R. Averbeck,[65] T. C. Awes,[54] B. Azmoun,[7] V. Babintsev,[24] M. Bai,[6] G. Baksay,[20] L. Baksay,[20] K. N. Barish,[8] B. Bassalleck,[51] A. T. Basye,[1] S. Bathe,[5,8] V. Baublis,[57] C. Baumann,[45] A. Bazilevsky,[7] S. Belikov,[7,*] R. Belmont,[13,44,69] R. Bennett,[65] A. Berdnikov,[61] Y. Berdnikov,[61] A. A. Bickley,[13] J. S. Bok,[52,73] K. Boyle,[65] M. L. Brooks,[39] H. Buesching,[7] V. Bumazhnov,[24] G. Bunce,[7,59] S. Butsyk,[39] C. M. Camacho,[39] S. Campbell,[65] C.-H. Chen,[65] C. Y. Chi,[14] M. Chiu,[7] I. J. Choi,[73] R. K. Choudhury,[4] P. Christiansen,[41] T. Chujo,[68] P. Chung,[64] O. Chvala,[8] V. Cianciolo,[54] Z. Citron,[65] B. A. Cole,[14] M. Connors,[65] P. Constantin,[39] M. Csanád,[18] T. Csörgő,[72] T. Dahms,[65] S. Dairaku,[35,58] I. Danchev,[69] K. Das,[21] A. Datta,[43] G. David,[7] A. Denisov,[24] A. Deshpande,[59,65] E. J. Desmond,[7] O. Dietzsch,[62] A. Dion,[65] M. Donadelli,[62] O. Drapier,[36] A. Drees,[65] K. A. Drees,[6] J. M. Durham,[39,65] A. Durum,[24] D. Dutta,[4] S. Edwards,[21] Y. V. Efremenko,[54] F. Ellinghaus,[13] T. Engelmore,[14] A. Enokizono,[38] H. En'yo,[58,59] S. Esumi,[68] B. Fadem,[46] D. E. Fields,[51] M. Finger,[9] M. Finger, Jr.,[9] F. Fleuret,[36] S. L. Fokin,[34] Z. Fraenkel,[71,*] J. E. Frantz,[53,65] A. Franz,[7] A. D. Frawley,[21] K. Fujiwara,[58] Y. Fukao,[58] T. Fusayasu,[48] I. Garishvili,[66] A. Glenn,[13] H. Gong,[65] M. Gonin,[36] Y. Goto,[58,59] R. Granier de Cassagnac,[36] N. Grau,[2,14] S. V. Greene,[69] M. Grosse Perdekamp,[25,59] Y. Gu,[64] T. Gunji,[12] H.-Å. Gustafsson,[41,*] J. S. Haggerty,[7] K. I. Hahn,[19] H. Hamagaki,[12] J. Hamblen,[66] R. Han,[56] J. Hanks,[14] E. P. Hartouni,[38] E. Haslum,[41] R. Hayano,[12] X. He,[22] M. Heffner,[38] T. K. Hemmick,[65] T. Hester,[8] J. C. Hill,[28] M. Hohlmann,[20] W. Holzmann,[14] K. Homma,[23] B. Hong,[33] T. Horaguchi,[23] D. Hornback,[66] S. Huang,[69] T. Ichihara,[58,59] R. Ichimiya,[58] J. Ide,[46] Y. Ikeda,[68] K. Imai,[29,35,58] M. Inaba,[68] D. Isenhower,[1] M. Ishihara,[58] T. Isobe,[12,58] M. Issah,[69] A. Isupov,[30] D. Ivanischev,[57] B. V. Jacak,[65] J. Jia,[7,64] J. Jin,[14] B. M. Johnson,[7] K. S. Joo,[47] D. Jouan,[55] D. S. Jumper,[1] F. Kajihara,[12] S. Kametani,[58] N. Kamihara,[59] J. Kamin,[65] J. H. Kang,[73] J. Kapustinsky,[39] K. Karatsu,[35,58] D. Kawall,[43,59] M. Kawashima,[58,60] A. V. Kazantsev,[34] T. Kempel,[28] A. Khanzadeev,[57] K. M. Kijima,[23] B. I. Kim,[33] D. H. Kim,[47] D. J. Kim,[31] E. Kim,[63] E.-J. Kim,[10] S. H. Kim,[73] Y.-J. Kim,[25] E. Kinney,[13] K. Kiriluk,[13] Á. Kiss,[18] E. Kistenev,[7] L. Kochenda,[57] B. Komkov,[57] M. Konno,[68] J. Koster,[25] D. Kotchetkov,[51] A. Kozlov,[71] A. Král,[15] A. Kravitz,[14] G. J. Kunde,[39] K. Kurita,[58,60] M. Kurosawa,[58] Y. Kwon,[73] G. S. Kyle,[52] R. Lacey,[64] Y. S. Lai,[14] J. G. Lajoie,[28] A. Lebedev,[28] D. M. Lee,[39] J. Lee,[19] K. Lee,[63] K. B. Lee,[33] K. S. Lee,[33] M. J. Leitch,[39] M. A. L. Leite,[62] E. Leitner,[69] B. Lenzi,[62] X. Li,[11] P. Liebing,[59] L. A. Linden Levy,[13] T. Liška,[15] A. Litvinenko,[30] H. Liu,[39,52] M. X. Liu,[39] B. Love,[69] R. Luechtenborg,[45] D. Lynch,[7] C. F. Maguire,[69] Y. I. Makdisi,[6] A. Malakhov,[30] M. D. Malik,[51] V. I. Manko,[34] E. Mannel,[14] Y. Mao,[56,58] H. Masui,[68] F. Matathias,[14] M. McCumber,[65] P. L. McGaughey,[39] N. Means,[65] B. Meredith,[25] Y. Miake,[68] A. C. Mignerey,[42] P. Mikeš,[9,27] K. Miki,[58,68] A. Milov,[7] M. Mishra,[3] J. T. Mitchell,[7] S. Mizuno,[58,68] A. K. Mohanty,[4] Y. Morino,[12] A. Morreale,[8] D. P. Morrison,[7,†] T. V. Moukhanova,[34] J. Murata,[58,60] S. Nagamiya,[32,58] J. L. Nagle,[13,‡] M. Naglis,[71] M. I. Nagy,[18] I. Nakagawa,[58,59] Y. Nakamiya,[23] T. Nakamura,[32] K. Nakano,[58,67] J. Newby,[38] M. Nguyen,[65] T. Niida,[68] R. Nouicer,[7] A. S. Nyanin,[34] E. O'Brien,[7] S. X. Oda,[12] C. A. Ogilvie,[28] M. Oka,[68] K. Okada,[59] Y. Onuki,[58] A. Oskarsson,[41] M. Ouchida,[23,58] K. Ozawa,[12] R. Pak,[7] V. Pantuev,[26,65] V. Papavassiliou,[52] I. H. Park,[19] J. Park,[63] S. K. Park,[33] W. J. Park,[33] S. F. Pate,[52] H. Pei,[28] J.-C. Peng,[25] H. Pereira,[16] V. Peresedov,[30] D. Yu. Peressounko,[34] C. Pinkenburg,[7] R. P. Pisani,[7] M. Proissl,[65] M. L. Purschke,[7] A. K. Purwar,[39] H. Qu,[22] J. Rak,[31] A. Rakotozafindrabe,[36] I. Ravinovich,[71] K. F. Read,[54,66] K. Reygers,[45] D. Reynolds,[64] V. Riabov,[50,57] Y. Riabov,[57] E. Richardson,[42] D. Roach,[69] G. Roche,[40] S. D. Rolnick,[8] M. Rosati,[28] C. A. Rosen,[13] S. S. E. Rosendahl,[41] P. Rosnet,[40] P. Rukoyatkin,[30] P. Ružička,[27] B. Sahlmueller,[45,65] N. Saito,[32] T. Sakaguchi,[7] K. Sakashita,[58,67] V. Samsonov,[50,57] S. Sano,[12,70] T. Sato,[68] S. Sawada,[32] K. Sedgwick,[8] J. Seele,[13] R. Seidl,[25] A. Yu. Semenov,[28] R. Seto,[8] D. Sharma,[71] I. Shein,[24] T.-A. Shibata,[58,67] K. Shigaki,[23] M. Shimomura,[49,68] K. Shoji,[35,58] P. Shukla,[4] A. Sickles,[7,25] C. L. Silva,[62] D. Silvermyr,[54] C. Silvestre,[16] K. S. Sim,[33] B. K. Singh,[3] C. P. Singh,[3] V. Singh,[3] M. Slunečka,[9] R. A. Soltz,[38] W. E. Sondheim,[39] S. P. Sorensen,[66] I. V. Sourikova,[7] N. A. Sparks,[1] P. W. Stankus,[54] E. Stenlund,[41] S. P. Stoll,[7] T. Sugitate,[23] A. Sukhanov,[7] J. Sziklai,[72] E. M. Takagui,[62] A. Taketani,[58,59] R. Tanabe,[68] Y. Tanaka,[48] K. Tanida,[35,58,59] M. J. Tannenbaum,[7] S. Tarafdar,[3] A. Taranenko,[50,64] P. Tarján,[17] H. Themann,[65] T. L. Thomas,[51] T. Todoroki,[58,68] M. Togawa,[35,58] A. Toia,[65] L. Tomášek,[27] H. Torii,[23] R. S. Towell,[1] I. Tserruya,[71] Y. Tsuchimoto,[23] C. Vale,[7,28] H. Valle,[69] H. W. van Hecke,[39] E. Vazquez-Zambrano,[14] A. Veicht,[25] J. Velkovska,[69] R. Vértesi,[17,72] A. A. Vinogradov,[34] M. Virius,[15] V. Vrba,[27] E. Vznuzdaev,[57] X. R. Wang,[52] D. Watanabe,[23] K. Watanabe,[68] Y. Watanabe,[58,59] F. Wei,[28] R. Wei,[64] J. Wessels,[45] S. N. White,[7] D. Winter,[14] J. P. Wood,[1] C. L. Woody,[7] R. M. Wright,[1] M. Wysocki,[13] W. Xie,[59] Y. L. Yamaguchi,[12] K. Yamaura,[23] R. Yang,[25] A. Yanovich,[24] J. Ying,[22] S. Yokkaichi,[58,59] Z. You,[56] G. R. Young,[54] I. Younus,[37,51] I. E. Yushmanov,[34] W. A. Zajc,[14] C. Zhang,[54] S. Zhou,[11] and L. Zolin[30]

(PHENIX Collaboration)

[1]*Abilene Christian University, Abilene, Texas 79699, USA*

[2]*Department of Physics, Augustana University, Sioux Falls, South Dakota 57197, USA*

[3]*Department of Physics, Banaras Hindu University, Varanasi 221005, India*

[4]*Bhabha Atomic Research Centre, Bombay 400 085, India*

[5]*Baruch College, City University of New York, New York, New York 10010, USA*

[6]*Collider-Accelerator Department, Brookhaven National Laboratory, Upton, New York 11973-5000, USA*

[7]*Physics Department, Brookhaven National Laboratory, Upton, New York 11973-5000, USA*

 ©2016 American Physical Society

[8]*University of California-Riverside, Riverside, California 92521, USA*
[9]*Charles University, Ovocný trh 5, Praha 1, 116 36 Prague, Czech Republic*
[10]*Chonbuk National University, Jeonju 561-756, Korea*
[11]*Science and Technology on Nuclear Data Laboratory, China Institute of Atomic Energy, Beijing 102413, People's Republic of China*
[12]*Center for Nuclear Study, Graduate School of Science, University of Tokyo, 7-3-1 Hongo, Bunkyo, Tokyo 113-0033, Japan*
[13]*University of Colorado, Boulder, Colorado 80309, USA*
[14]*Columbia University, New York, New York 10027, USA and Nevis Laboratories, Irvington, New York 10533, USA*
[15]*Czech Technical University, Zikova 4, 166 36 Prague 6, Czech Republic*
[16]*Dapnia, CEA Saclay, F-91191 Gif-sur-Yvette, France*
[17]*Debrecen University, H-4010 Debrecen, Egyetem tér 1, Hungary*
[18]*ELTE, Eötvös Loránd University, H-1117 Budapest, Pázmany Péter sétány 1/A, Hungary*
[19]*Ewha Womans University, Seoul 120-750, Korea*
[20]*Florida Institute of Technology, Melbourne, Florida 32901, USA*
[21]*Florida State University, Tallahassee, Florida 32306, USA*
[22]*Georgia State University, Atlanta, Georgia 30303, USA*
[23]*Hiroshima University, Kagamiyama, Higashi-Hiroshima 739-8526, Japan*
[24]*IHEP Protvino, State Research Center of Russian Federation, Institute for High Energy Physics, Protvino 142281, Russia*
[25]*University of Illinois at Urbana-Champaign, Urbana, Illinois 61801, USA*
[26]*Institute for Nuclear Research of the Russian Academy of Sciences, prospekt 60-letiya Oktyabrya 7a, Moscow 117312, Russia*
[27]*Institute of Physics, Academy of Sciences of the Czech Republic, Na Slovance 2, 182 21 Prague 8, Czech Republic*
[28]*Iowa State University, Ames, Iowa 50011, USA*
[29]*Advanced Science Research Center, Japan Atomic Energy Agency, 2-4 Shirakata Shirane, Tokai-mura, Naka-gun, Ibaraki-ken 319-1195, Japan*
[30]*Joint Institute for Nuclear Research, 141980 Dubna, Moscow Region, Russia*
[31]*Helsinki Institute of Physics, University of Jyväskylä, P.O. Box 35, FI-40014 Jyväskylä, Finland*
[32]*KEK, High Energy Accelerator Research Organization, Tsukuba, Ibaraki 305-0801, Japan*
[33]*Korea University, Seoul 136-701, Korea*
[34]*National Research Center "Kurchatov Institute," Moscow 123098, Russia*
[35]*Kyoto University, Kyoto 606-8502, Japan*
[36]*Laboratoire Leprince-Ringuet, Ecole Polytechnique, CNRS-IN2P3, Route de Saclay, F-91128 Palaiseau, France*
[37]*Department of Physics, Lahore University of Management Sciences, Lahore 54792, Pakistan*
[38]*Lawrence Livermore National Laboratory, Livermore, California 94550, USA*
[39]*Los Alamos National Laboratory, Los Alamos, New Mexico 87545, USA*
[40]*LPC, Université Blaise Pascal, CNRS-IN2P3, Clermont-Fd, 63177 Aubiere Cedex, France*
[41]*Department of Physics, Lund University, Box 118, SE-221 00 Lund, Sweden*
[42]*University of Maryland, College Park, Maryland 20742, USA*
[43]*Department of Physics, University of Massachusetts, Amherst, Massachusetts 01003-9337, USA*
[44]*Department of Physics, University of Michigan, Ann Arbor, Michigan 48109-1040, USA*
[45]*Institut für Kernphysik, University of Muenster, D-48149 Muenster, Germany*
[46]*Muhlenberg College, Allentown, Pennsylvania 18104-5586, USA*
[47]*Myongji University, Yongin, Kyonggido 449-728, Korea*
[48]*Nagasaki Institute of Applied Science, Nagasaki-shi, Nagasaki 851-0193, Japan*
[49]*Nara Women's University, Kita-uoya Nishi-machi Nara 630–8506, Japan*
[50]*National Research Nuclear University, MEPhI, Moscow Engineering Physics Institute, Moscow 115409, Russia*
[51]*University of New Mexico, Albuquerque, New Mexico 87131, USA*
[52]*New Mexico State University, Las Cruces, New Mexico 88003, USA*
[53]*Department of Physics and Astronomy, Ohio University, Athens, Ohio 45701, USA*
[54]*Oak Ridge National Laboratory, Oak Ridge, Tennessee 37831, USA*
[55]*IPN-Orsay, Université Paris-Sud, CNRS/IN2P3, Université Paris-Saclay, BP1, F-91406 Orsay, France*
[56]*Peking University, Beijing 100871, People's Republic of China*
[57]*PNPI, Petersburg Nuclear Physics Institute, Gatchina, Leningrad Region 188300, Russia*
[58]*RIKEN Nishina Center for Accelerator-Based Science, Wako, Saitama 351-0198, Japan*
[59]*RIKEN BNL Research Center, Brookhaven National Laboratory, Upton, New York 11973-5000, USA*
[60]*Department of Physics, Rikkyo University, 3-34-1 Nishi-Ikebukuro, Toshima, Tokyo 171-8501, Japan*
[61]*Saint Petersburg State Polytechnic University, St. Petersburg, 195251 Russia*
[62]*Universidade de São Paulo, Instituto de Física, Caixa Postal 66318, São Paulo CEP05315-970, Brazil*
[63]*Department of Physics and Astronomy, Seoul National University, Seoul 151-742, Korea*
[64]*Department of Chemistry, Stony Brook University, SUNY, Stony Brook, New York 11794-3400, USA*
[65]*Department of Physics and Astronomy, Stony Brook University, SUNY, Stony Brook, New York 11794-3800, USA*

[66]*University of Tennessee, Knoxville, Tennessee 37996, USA*
[67]*Department of Physics, Tokyo Institute of Technology, Oh-okayama, Meguro, Tokyo 152-8551, Japan*
[68]*Center for Integrated Research in Fundamental Science and Engineering, University of Tsukuba, Tsukuba, Ibaraki 305, Japan*
[69]*Vanderbilt University, Nashville, Tennessee 37235, USA*
[70]*Waseda University, Advanced Research Institute for Science and Engineering, 17 Kikui-cho, Shinjuku-ku, Tokyo 162-0044, Japan*
[71]*Weizmann Institute, Rehovot 76100, Israel*
[72]*Institute for Particle and Nuclear Physics, Wigner Research Centre for Physics, Hungarian Academy of Sciences (Wigner RCP, RMKI) H-1525 Budapest 114, P.O. Box 49, Budapest, Hungary*
[73]*Yonsei University, IPAP, Seoul 120-749, Korea*

(Received 3 December 2014; revised manuscript received 13 July 2015; published 31 May 2016)

Measurements of the anisotropic flow coefficients $v_2\{\Psi_2\}$, $v_3\{\Psi_3\}$, $v_4\{\Psi_4\}$, and $v_4\{\Psi_2\}$ for identified particles ($\pi^\pm$, $K^\pm$, and $p+\bar{p}$) at midrapidity, obtained relative to the event planes Ψ_m at forward rapidities in Au + Au collisions at $\sqrt{s_{NN}} = 200$ GeV, are presented as a function of collision centrality and particle transverse momenta p_T. The v_n coefficients show characteristic patterns consistent with hydrodynamical expansion of the matter produced in the collisions. For each harmonic n, a modified valence quark-number N_q scaling [plotting $v_n\{\Psi_m\}/(N_q)^{n/2}$ versus transverse kinetic energies $(\mathrm{KE}_T)/N_q$] is observed to yield a single curve for all the measured particle species for a broad range of KE_T. A simultaneous blast-wave model fit to the observed $v_n\{\Psi_m\}(p_T)$ coefficients and published particle spectra identifies radial flow anisotropies $\rho_n\{\Psi_m\}$ and spatial eccentricities $s_n\{\Psi_m\}$ at freeze-out. These are generally smaller than the initial-state participant-plane geometric eccentricities $\varepsilon_n\{\Psi_m^{\mathrm{PP}}\}$ as also observed in the final eccentricity from quantum interferometry measurements with respect to the event plane.

DOI: 10.1103/PhysRevC.93.051902

Introduction. The quark-gluon plasma (QGP) is a novel phase of nuclear matter at high temperatures and energy density, whose existence is predicted by quantum chromodynamics [1]. A wide variety of experimental observations at the Relativistic Heavy Ion Collider (RHIC) [2–5] provides strong evidence for the formation of a QGP in ultrarelativistic heavy ion collisions, particularly (1) the magnitude of the observed suppression of high-p_T ($p_T \gtrsim 4$ GeV/c) particles, relative to the scaled yield from $p+p$ collisions and (2) the large azimuthal anisotropy or anisotropic flow of the low-p_T ($p_T \lesssim 3$ to 4 GeV/c) bulk of hadrons (HADs) in the final state. The flow of low-p_T particles has been attributed to anisotropic expansion of the QGP [6–8], and consequently the measured strength of anisotropic flow should be sensitive to the transport properties of the QGP and the mechanism for its space-time evolution.

The magnitude of anisotropic flow can be quantified by the Fourier coefficients $v_n\{\Psi_m\} = \langle\cos[n(\phi-\Psi_m)]\rangle$ of the azimuthal distribution of produced particles [9–12], where n and m are the order of the harmonics, ϕ is the azimuthal angle of the particles, and Ψ_m is the azimuthal angle of the mth-order event plane (EP). In early studies with symmetric systems, $v_n\{\Psi_m\}$ was presumed to be zero for odd n owing to the assumption that initial-state energy densities were smooth and symmetric across the transverse plane. The recent observations of sizable $v_n\{\Psi_n\}$ values for odd n [13–17] confirm the important role of fluctuations in the initial-state collision geometry [18].

Model-dependent analyses of higher-order harmonics for inclusive hadrons measured in Au + Au and Pb + Pb collisions at RHIC and the Large Hadron Collider have indicated that such measurements can provide simultaneous constraints for initial-state fluctuation models and the ratio of shear viscosity to entropy density of the QGP [8,13,19,20]. The new data on higher-order $v_n\{\Psi_m\}$ for identified particles presented here provide additional information about the initial conditions and hydrodynamic properties. Here, we show that our $v_n\{\Psi_m\}$ measurements for different particle species provide (1) further tests for the constituent quark-number scaling and quark coalescence models [21–23] by extending our previously observed scaling for $v_2\{\Psi_2\}$ [24,25] to higher harmonics [26] and (2) freeze-out parameters for hydrodynamic expansion with anisotropic blast-wave (BW) model fits [27–30].

Data taking and particle identification. The results presented here for Au + Au collisions at $\sqrt{s_{NN}} = 200$ GeV are obtained with the PHENIX Collaboration's experiment from an analysis of 4.14×10^9 minimum-bias events taken during the 2007 running period. Collision centrality is determined with the beam-beam counters [31]. Charged hadrons are reconstructed in a pseudorapidity (η) range of $|\eta| < 0.35$ using the drift-chamber and pad-chamber subsystems [32], which achieve the momentum resolution $\delta p/p \approx 1.3\% \oplus 1.2\% \times p$ (GeV/c) [33]. The ring imaging Čerenkov counter is employed to veto conversion electrons. Time-of-flight detectors in both the east [(TOFE), $\Delta\varphi = \pi/4$ rad] and the west [(TOFW), $\Delta\varphi = 0.342$ rad] arms are used for $\pi^\pm$, $K^\pm$, and $p+\bar{p}$ identification after the conversion electron veto [33]. The timing resolution of TOFE (TOFW) is 133 (84 ± 1) ps. For $p_T < 3$ GeV/c, both TOFE and TOFW detectors were used. For $p_T > 3$ GeV/c particle identification utilizes the TOFW in conjunction with the aerogel Čerenkov counter. The two detectors have a common azimuthal acceptance of

*Deceased.
†PHENIX cospokesperson. morrison@bnl.gov
‡PHENIX cospokesperson. jamie.nagle@colorado.edu

$\Delta\varphi = 0.171$ rad. With these detectors, a $p + \bar{p}$ purity of greater than 97% was achieved for $p_T < 4$ GeV/c; and purities for $\pi^{\pm}$ and $K^{\pm}$ greater than 98% for $p_T < 3$ GeV/c and 90% for $3 < p_T < 4$ GeV/c were also achieved as detailed in Ref. [33]. The purity and efficiency of particle identification (PID) are independent of the relative azimuthal angle between the particles and the event plane $\phi - \Psi_m$.

Experimental technique. Measurements of the flow coefficients $v_2\{\Psi_2\}$, $v_3\{\Psi_3\}$, $v_4\{\Psi_4\}$, and $v_4\{\Psi_2\}$ as a function of centrality and p_T for $\pi^{\pm}$, $K^{\pm}$, and $p + \bar{p}$ (i.e., with charge signs combined) are obtained with both the EP and the long-range two-particle correlation (2PC) methods. In the EP method, a measured event-plane direction $\Psi_m^{\rm obs}$ is determined for every event and for each order m using the south and north reaction-plane detectors (RXN), covering $\Delta\varphi = 2\pi$ and $1 < |\eta| < 2.8$ [34]. Each is made of plastic scintillator paddles with lead converters in front and with optical fibers guided to photomultiplier tubes. Each RXN detector is segmented into 12 sections in φ and two rings in η. The $\Psi_m^{\rm obs}$'s are determined via a sum over the azimuthal angle ϕ_i of each RXN element in both the arms with its charge w_i deposited by particles for that event as $\tan(m\Psi_m^{\rm obs}) = \sum_i w_i \sin(m\phi_i)/\sum_i w_i \cos(m\phi_i)$. The flow magnitudes $v_n\{\Psi_m\} = \langle\cos n(\phi - \Psi_m^{\rm obs})\rangle/{\rm Res}\{n,\Psi_m\}$ are then measured with respect to each harmonic event plane, where ϕ is the azimuthal angle of the hadron and ${\rm Res}\{n,\Psi_m\} = \langle\cos n(\Psi_m - \Psi_m^{\rm obs})\rangle$ is the event plane resolution, which is estimated for each centrality by the standard subevent method as described in Refs. [10,35,36]. The best resolution of each harmonic is measured to be ${\rm Res}\{2,\Psi_2\} \sim 0.75$ and ${\rm Res}\{4,\Psi_2\} \sim 0.5$ (${\rm Res}\{3,\Psi_3\} \sim 0.3$ and ${\rm Res}\{4,\Psi_4\} \sim 0.15$) in 20%–30% (0%–10%) central collisions.

The 2PC method pairs the HADs with deposited charges in the RXN segments. The distribution of the relative azimuthal angles of particle hits in separate η ranges A and $B, \Delta\phi \equiv \phi^A - \phi^B$ reflects the product of the v_n's via $dN/d\,\Delta\phi \propto 1 + \sum_{n=1} 2v_n^A v_n^B \cos(n\,\Delta\phi)$ [10,37,38]. We analyze the $\Delta\phi$ correlations using the mixed-event technique for two pair combinations $(A,B) = ({\rm HAD,RXN})$ and $(A,B) = ({\rm RXN\text{-}N,RXN\text{-}S})$. These correlations then fix the event-averaged products $\langle v_n^{\rm HAD} v_n^{\rm RXN}\rangle$ and $\langle v_n^{\rm RXN} v_n^{\rm RXN}\rangle$ and allow us to obtain $v_n^{\rm HAD} = \langle v_n^{\rm HAD} v_n^{\rm RXN}\rangle/\sqrt{\langle v_n^{\rm RXN} v_n^{\rm RXN}\rangle}$. Note that flow harmonics extracted with the 2PC method are not measured with respect to event planes. Thus, from this point forward we refer to flow harmonics in the 2PC methods as $v_n\{2{\rm PC}\}$. We use v_n in cases when the discussion is generically about either method. In both of the analysis methods used, the results for wider centrality ranges are obtained by averaging across several smaller ranges, weighted by the multiplicity of the selected particle [39].

The systematic uncertainties in the v_n measurements were estimated for: (1) η acceptance variation of the RXNs in the EP and 2PC methods; this is correlated among $v_n(p_T)$'s for each hadron species with the same fractional v_n amount in the entire p_T range, except for $v_4\{\Psi_4\}$ where it tends to decrease as p_T increases; (2) detector acceptance effects of TOFE and TOFW, including occupancy; these are correlated among $v_n(p_T)$'s for each hadron species with the same v_n constant in the entire p_T range; (3) hadron track-hit matching cut; and (4) particle identification purity. The systematic uncertainties (1) and (2) are p_T correlated, whereas (3) and (4) are p_T uncorrelated. These uncertainties are similar between the EP and the 2PC methods. Table I summarizes typical systematic uncertainties on the different $v_n\{\Psi_m\}$ measures in the EP method for $\pi^{\pm}$ at $p_T = 2$ GeV/c.

TABLE I. Systematic uncertainties on the measured $v_n\{\Psi_m\}$ by the EP method for $\pi^{\pm}$ at $p_T = 2$ GeV/c in 0%–10% (30%–50%) central collisions. Uncertainties of type (2) are absolute in the $v_n\{\Psi_m\}$ value with the multiplication factor 10^{-3}; the others are relative fractions of $v_n\{\Psi_m\}$ expressed in percentages.

Type	Source	$v_2\{\Psi_2\}$	$v_3\{\Psi_3\}$	$v_4\{\Psi_4\}$	$v_4\{\Psi_2\}$
(1)	RXN η (%)	4.3(3.0)	4.7(12.5)	16(31)	34(7.0)
(2)	Acceptance [10^{-3}]	5.0(1.0)	0.5(2.0)	0.7(2.5)	0.1(0.2)
(3)	Matching (%)	1.4(0.3)	0.7(1.0)	2.6(2.8)	7.7(1.7)
(4)	PID (%)	0.3(0.1)	0.3(0.3)	0.8(1.0)	2.7(0.4)

Results for the 0%–50% centrality bin. Figures 1(a)–1(c) show a comparison of $v_2(p_T)$, $v_3(p_T)$, and $v_4(p_T)$ for $\pi^{\pm}$, $K^{\pm}$, and $p + \bar{p}$ for the EP (solid points) and 2PC (open points) methods in a 0%–50% centrality sample; they indicate very good agreement between the two methods. Shown in Fig. 1(d) is $v_4\{\Psi_2\}$, i.e., the fourth harmonic coefficient with respect to the second-order harmonic event plane. It can be seen that $v_4\{\Psi_2\}$ is smaller than $v_4\{\Psi_4\}$ but still sizable, indicating significant correlations between Ψ_2 and Ψ_4 [40], which can be ascertained through the trigonometric identity $v_4\{\Psi_2\}/v_4\{\Psi_4\} = \langle\cos 4(\Psi_2 - \Psi_4)\rangle$ [41]. There are two trends common to all n's in Fig. 1: (1) in the low-p_T region the anisotropy appears largest for the lightest hadron and

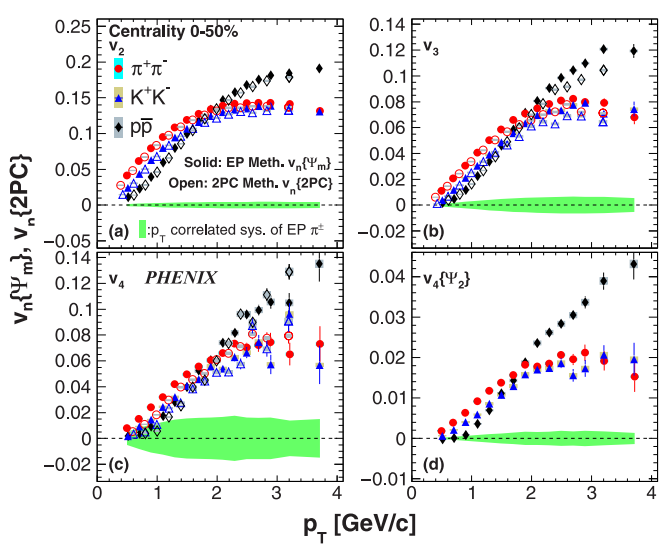

FIG. 1. Fourier coefficients for charge-combined $\pi^{\pm}$, $K^{\pm}$, and $p + \bar{p}$ at midrapidity for 0%–50% central Au + Au collisions at $\sqrt{s_{NN}} = 200$ GeV. Different p_T bins were used for the EP and 2PC methods. The green bands indicate the p_T -correlated systematic uncertainties of the $\pi^{\pm}$ results from the EP method. The shaded boxes around the data points are p_T -uncorrelated systematic uncertainties, which are smaller than the symbols in many cases.

smallest for the heaviest hadron, and (2) in the intermediate-p_T ($3 \lesssim p_T \lesssim 4$-GeV/$c$) region this mass dependence partly reverses such that the anisotropy is greater for the baryons ($N_q = 3$) than for the mesons ($N_q = 2$) at the same p_T. These trends remain significant after taking into account the p_T -correlated systematic uncertainties. These patterns have been observed previously in $v_2\{\Psi_2\}$ measurements for identified particles in Au + Au collisions at RHIC [29,33] and are seen here to hold for the higher moments $v_3\{\Psi_3\}$, $v_4\{\Psi_4\}$, and $v_4\{\Psi_2\}$. The mass dependence in the low-p_T range is a generic feature of hydrodynamical models, reflecting the mass ordering from the common velocity field (i.e., radial flow), and the dependence on valence quark number in the intermediate-p_T region has been associated with the development of flow in the partonic phase [24].

Results for finer centrality bins. The $v_n\{\Psi_m\}$ of $\pi^\pm$, $K^\pm$, and $p + \bar{p}$ measured with the event-plane method are shown in Fig. 2 for the centrality selections 0%–10% and 30%–50%. The same mass dependence of $v_n\{\Psi_m\}$ is seen in the low-p_T region for all harmonics and centralities. The evolution of baryon-meson splitting at intermediate p_T is also observed for all centralities in $v_2\{\Psi_2\}$ and $v_3\{\Psi_3\}$ but could not be confirmed for $v_4\{\Psi_4\}$ in the most-central and more peripheral events or for $v_4\{\Psi_2\}$ in the most-central events owing to the lower statistical significance of the measurements in those bins.

Quark-number scaling. The baryon-meson splitting in the intermediate-p_T region can be taken as an indication that the number of constituent valence quarks N_q is an important determinant of final-state hadron flow in this range. Indeed, the $v_2\{\Psi_2\}$ data for identified hadrons had previously been seen to scale such that $v_2\{\Psi_2\}/N_q$ was the same for different particle species when evaluated at the same transverse kinetic energy (KE_T) per constituent quark number in the range of $\mathrm{KE}_T/N_q \lesssim 1$ GeV ($\mathrm{KE}_T \equiv m_T - m_0$ and $m_T \equiv \sqrt{p_T{}^2 + m_0^2}$, where m_0 is the hadron mass), i.e., "quark-number scaling" [24,33]. We have found that the present data obey a generalization of this scaling [26] where for each harmonic order n, the values of $v_n\{\Psi_m\}/(N_q)^{n/2}$ versus KE_T/N_q lie on a single curve for all the measured species within a ±15% range. Figure 3 shows the adherence of the data to this empirical scaling, which reflects the combination of quark-number scaling for $v_2\{\Psi_2\}$ by quark coalescence [42] and the empirical observation $v_n\{\Psi_n\}(p_T) \propto [v_2\{\Psi_2\}(p_T)]^{n/2}$ [15]. Any explanation of the underlying physics needs to match this scaling over this KE_T range, and neither hydrodynamics [11,20,43,44] nor naive quark coalescence alone [45] predicts this scaling for the higher moments. It is notable that, for $v_2\{\Psi_2\}$, there are deviations from valence-quark scaling at higher p_T with mesons and baryons having comparable anisotropies [33]. Reconciling the different physics as a function of p_T remains an outstanding challenge.

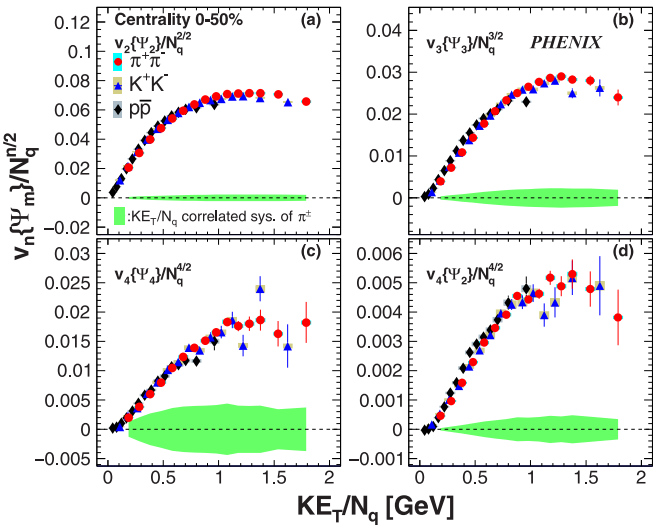

FIG. 3. Quark-number (N_q) scaling for 0%–50% central Au + Au collisions at $\sqrt{s_{NN}} = 200$ GeV, where N_q is the constituent valence quark number of each hadron. Systematic uncertainties are shown as in Fig. 1.

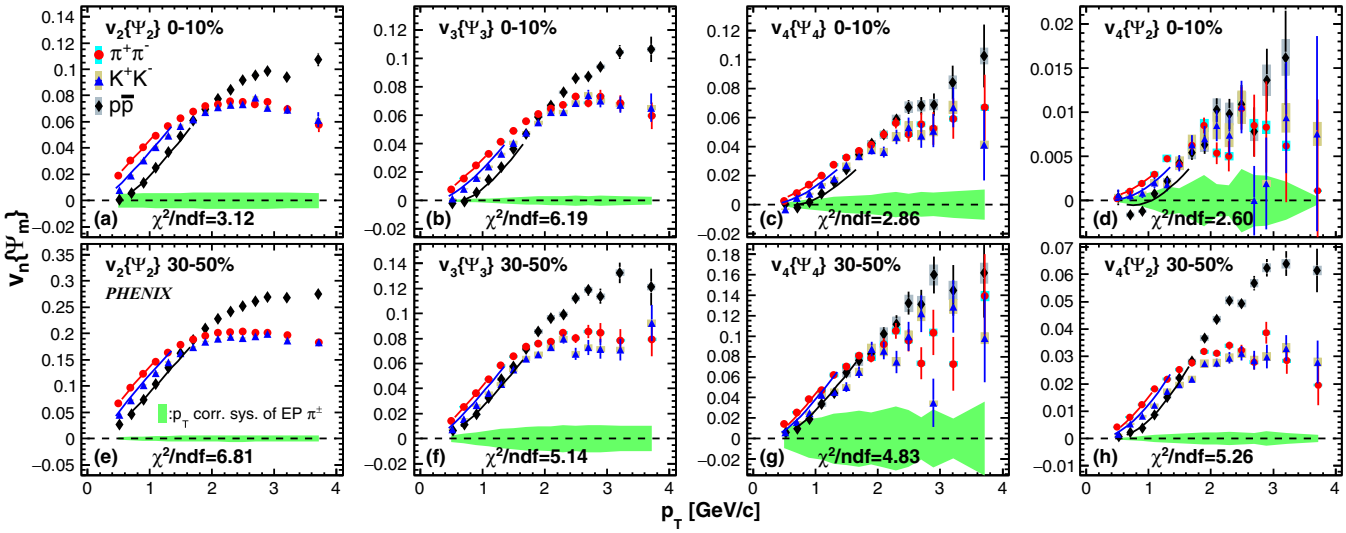

FIG. 2. Fourier coefficients for charge-combined $\pi^\pm$, $K^\pm$, and $p + \bar{p}$ at midrapidity in Au + Au collisions at $\sqrt{s_{NN}} = 200$ GeV. Coefficients are determined using the event-plane method. The curves illustrate the fits from the BW model. Systematic uncertainties are shown as in Fig. 1.

Blast-wave fitting. The BW model [27–30] is a description of a fluid freeze-out state characterized by its temperature T_f and its ϕ-averaged maximal radial flow rapidity ρ_0. Here we extend the BW description to incorporate azimuthal anisotropies in both radial rapidities $\rho_n\{\Psi_m\}$ and spatial density $s_n\{\Psi_m\}$ for $n = 2$–4 using the empirically defined quantities $\rho(n,m,\phi,r) = \rho_0[1 + 2\rho_n\{\Psi_m\}\cos(n\phi)] \times r/R^{\max}$ and $S(n,m,\phi) = 1 + 2s_n\{\Psi_m\}\cos(n\phi)$. The spectra and anisotropies of all hadrons freezing out of the fluid can then be predicted via [28,29]

$$\frac{dN}{p_T dp_T} \propto \int^{R^{\max}} r\,dr \int d\phi\; m_T I_0(\alpha_t) K_1(\beta_t),$$
$$v_n\{\Psi_m\} = \frac{\int^{R^{\max}} r\,dr \int d\phi\, \cos(n\phi) I_n(\alpha_t) K_1(\beta_t) S(n,m,\phi)}{\int^{R^{\max}} r\,dr \int d\phi\, I_0(\alpha_t) K_1(\beta_t) S(n,m,\phi)}, \tag{1}$$

where I_n and K_1 are modified Bessel functions of the first and second kinds, $\alpha_t = (p_T/T_f)\sinh\rho(n,m,\phi,r)$, and $\beta_t = (m_T/T_f)\cosh\rho(n,m,\phi,r)$. Using single-particle spectra from Ref. [46] together with the present $v_n\{\Psi_m\}$ data, BW parameters $T_f, \rho_0, \rho_n\{\Psi_m\}$ and $s_n\{\Psi_m\}$ are extracted via simultaneous fitting of the $\pi^\pm$, $K^\pm$, and $p + \bar{p}$ data with a minimization of global χ^2, separately for each centrality selection and each $v_n\{\Psi_m\}$. The fit ranges used for the $\pi^\pm$, $K^\pm$, and $p + \bar{p}$ are $0.5 < p_T < 1.1$ GeV/c, $0.4 < p_T < 1.3$ GeV/c, and $0.6 < p_T < 1.7$ GeV/c, respectively. The BW fits to $v_n\{\Psi_m\}(p_T)$ + spectra are compared to the data in Fig. 2 for 0%–10% and 30%–50% central collisions, together with the global $\chi^2/n\,df$ of the fits determined using the quadrature sum of the statistical and systematic uncertainties of the data. The global $\chi^2/n\,df$ in 10%–20% and 20%–30% central collisions is similar to that in 0%–10% and 30%–50% central collisions.

The results for the BW parameters are shown in Fig. 4. The freeze-out temperatures T_f and radially averaged flow rapidities $\langle\rho\rangle = \int[\rho_0 \times r/R_{\max}]r\,dr/\int r\,dr$ are in good agreement for the fits at different n's as would be required for a model of freeze-out. T_f and $\langle\rho\rangle$ are primarily determined by the single-particle spectra [47], whereas $\rho_n\{\Psi_m\}$ and $s_n\{\Psi_m\}$ are determined by $v_n\{\Psi_m\}$ measurements including p_T and particle mass dependences.

The radial rapidity and spatial density anisotropies $\rho_n\{\Psi_m\}$ and $s_n\{\Psi_m\}$ extracted from the fits are shown against the average initial-state spatial participant-plane (PP) anisotropy $\varepsilon_n\{\Psi_m^{\rm PP}\} = \langle\{r^2\cos n(\phi^{\rm part} - \Psi_m^{\rm PP})\}/\{r^2\}\rangle$, where r and $\phi^{\rm part}$ are the polar coordinate positions of collision participant nucleons defined by Glauber models [18,48] and $\Psi_m^{\rm PP}$ is the angle determined as $\tan(m\Psi_m^{\rm PP}) = \{r^2\sin m\phi^{\rm part}\}/\{r^2\cos m\phi^{\rm part}\}$. Here, the brackets $\langle\,\rangle$ and $\{\,\}$ denote averages over events and participants, respectively. The amplitude of $\varepsilon_n\{\Psi_m^{\rm PP}\}$ is smallest for the most-central collisions and increases with centrality percentile.

Eccentricity of the medium at freeze-out. The $\rho_n\{\Psi_m\}$ and $s_n\{\Psi_m\}$ are generally smaller than the $\varepsilon_n\{\Psi_m^{\rm PP}\}$. The $\rho_n\{\Psi_m\}$ has a positive finite value and generally follows a common increasing curve as a function of $\varepsilon_n\{\Psi_m^{\rm PP}\}$ for $n = 2$–4. The $s_2\{\Psi_2\}$, $s_3\{\Psi_3\}$, and $s_4\{\Psi_4\}$ also show a common increasing trend in $\varepsilon_n\{\Psi_m^{\rm PP}\} \gtrsim 0.1$. We can interpret relative oscillations

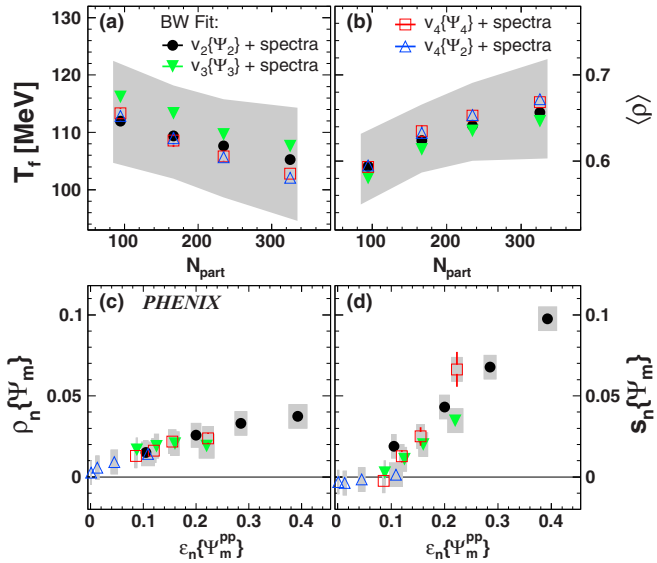

FIG. 4. BW model fit parameters extracted for each $v_n\{\Psi_m\}$ + spectrum across different centrality classes. The gray bands in (a) and (b) and shaded boxes in (c) and (d) indicate systematic uncertainties on the fitting p_T range and those propagated from the measurements. The width of the shaded boxes in the $\varepsilon_n\{\Psi_m^{\rm PP}\}$ direction in (c) and (d) indicates systematic uncertainties from Glauber models. Systematic uncertainties in (a) and (b) are similar among different fittings.

of event-plane-dependent Hanbury-Brown-Twiss (HBT) radii with respect to averaged radii as the eccentricity of the medium at freeze-out if the direction of the radii is selected perpendicular to beam and pair momentum ($R_{\rm side}$) where these radii are less influenced by the emission duration and position-momentum correlations [49].

Spatial information. Finite final eccentricities for $n = 2$ and $n = 3$ are observed by both the BW fit to $v_n\{\Psi_m\}$ and the event-plane-dependent HBT radii measurements using positive and negative pion pairs [49]. The $s_n\{\Psi_m\}$ therefore could reflect physical effects at the freeze-out of the medium. The finite $s_n\{\Psi_m\}$ could be interpreted as a residual effect of initial-state anisotropy $\varepsilon_n\{\Psi_m^{\rm PP}\}$, especially the contribution of initial-state fluctuations for $n = 3,4$ after its dilution by the medium expansion. For $\varepsilon_n\{\Psi_m^{\rm PP}\} \lesssim 0.1$, $s_3\{\Psi_3\}$, $s_4\{\Psi_4\}$, and $s_4\{\Psi_2\}$ are consistent with zero within systematic uncertainties. Comparisons of these small $s_n\{\Psi_m\}$ to the finite $\rho_n\{\Psi_m\}$ and $v_n\{\Psi_m\}$ in this $\varepsilon_n\{\Psi_m^{\rm PP}\}$ range indicate that the anisotropic expansion velocity $\rho_n\{\Psi_m\}$ is a dominant source of the observed $v_n\{\Psi_m\}$ for higher harmonics. We expect this spatial information could provide new insights into freeze-out conditions in hydrodynamic calculations.

Summary and conclusions. To summarize, the anisotropy strengths $v_2\{\Psi_2\}$, $v_3\{\Psi_3\}$, $v_4\{\Psi_4\}$, and $v_4\{\Psi_2\}$ for $\pi^\pm$, $K^\pm$, and $p + \bar{p}$ produced at midrapidity in Au + Au collisions at RHIC have been presented. The higher-order harmonics $v_n\{\Psi_m\}$ show a particle mass splitting at low p_T and a baryon-meson difference at intermediate p_T, very similar to what has been seen already for $v_2\{\Psi_2\}$. The anisotropies obey a modified quark-number scaling, where $v_n\{\Psi_m\}/(N_q)^{n/2}$ falls on a common trend against ${\rm KE}_T/N_q$ for each n. The data can

be fit with a generalized BW model with empirically defined anisotropies in radial rapidity and spatial density at higher harmonic orders, which could provide a geometrical view of the hydrodynamical expansion at the end of freeze-out. Future analyses combining the results in this Rapid Communication with similar results from HBT and jetlike correlations with respect to higher-order event planes will further constrain the conditions and properties of the matter created at RHIC.

Acknowledgments. We thank the staff of the Collider-Accelerator and Physics Departments at Brookhaven National Laboratory and the staff of the other PHENIX Collaboration participating institutions for their vital contributions. We acknowledge support from the Office of Nuclear Physics in the Office of Science of the Department of Energy, the National Science Foundation, Abilene Christian University Research Council, Research Foundation of SUNY, and Dean of the College of Arts and Sciences, Vanderbilt University (USA), Ministry of Education, Culture, Sports, Science, and Technology and the Japan Society for the Promotion of Science (Japan), Conselho Nacional de Desenvolvimento Científico e Tecnológico and Fundação de Amparo à Pesquisa do Estado de São Paulo (Brazil), Natural Science Foundation of China (People's Republic of China), Ministry of Education, Youth and Sports (Czech Republic), Centre National de la Recherche Scientifique, Commissariat à l'Énergie Atomique, and Institut National de Physique Nucléaire et de Physique des Particules (France), Bundesministerium für Bildung und Forschung, Deutscher Akademischer Austausch Dienst, and Alexander von Humboldt Stiftung (Germany), National Science Fund, OTKA, Károly Róbert University College, the Ch. Simonyi Fund (Hungary), Department of Atomic Energy and Department of Science and Technology (India), Israel Science Foundation (Israel), Basic Science Research Program through NRF of the Ministry of Education (Korea), Physics Department, Lahore University of Management Sciences (Pakistan), Ministry of Education and Science, Russian Academy of Sciences, Federal Agency of Atomic Energy (Russia), VR and Wallenberg Foundation (Sweden), the U.S. Civilian Research and Development Foundation for the Independent States of the Former Soviet Union, the U.S.-Hungarian Fulbright Foundation for Educational Exchange, and the U.S.-Israel Binational Science Foundation.

[1] E. V. Shuryak, Nonperturbative phemomena in QCD vacuum, hadrons, and quark-gluon plasma, CERN Yellow Report 83-01, Geneva (1983).

[2] I. Arsene *et al.* (BRAHMS Collaboration), Quark gluon plasma and color glass condensate at RHIC? The Perspective from the BRAHMS experiment, Nucl. Phys. A **757**, 1 (2005).

[3] B. B. Back, M. D. Baker, M. Ballintijn, D.S. Barton, B. Becker *et al.*, The PHOBOS perspective on discoveries at RHIC, Nucl. Phys. A **757**, 28 (2005).

[4] John Adams *et al.* (STAR Collaboration), Experimental and theoretical challenges in the search for the quark gluon plasma: The STAR Collaboration's critical assessment of the evidence from RHIC collisions, Nucl. Phys. A **757**, 102 (2005).

[5] K. Adcox *et al.* (PHENIX Collaboration), Formation of dense partonic matter in relativistic nucleus-nucleus collisions at RHIC: Experimental evaluation by the PHENIX Collaboration, Nucl. Phys. A **757**, 184 (2005).

[6] H. Song, S. A. Bass, U. Heinz, T. Hirano, and C. Shen, 200 A GeV Au+Au Collisions Serve a Nearly Perfect Quark-Gluon Liquid, Phys. Rev. Lett. **106**, 192301 (2011).

[7] G. S. Denicol, T. Kodama, and T. Koide, The effect of shear and bulk viscosities on elliptic flow, J. Phys. G: Nucl. Part. Phys. **37**, 094040 (2010).

[8] B. Schenke, S. Jeon, and C. Gale, Higher flow harmonics from (3+1)D event-by-event viscous hydrodynamics, Phys. Rev. C **85**, 024901 (2012).

[9] S. Voloshin and Y. Zhang, Flow study in relativistic nuclear collisions by Fourier expansion of Azimuthal particle distributions, Z. Phys. C **70**, 665 (1996).

[10] A. M. Poskanzer and S. A. Voloshin, Methods for analyzing anisotropic flow in relativistic nuclear collisions, Phys. Rev. C **58**, 1671 (1998).

[11] J.-Y. Ollitrault, Anisotropy as a signature of transverse collective flow, Phys. Rev. D **46**, 229 (1992).

[12] A. Adare *et al.* (PHENIX Collaboration), Elliptic and Hexadecapole Flow of Charged hadrons in Au+Au collisions at $\sqrt{s_{NN}} = 200$ GeV, Phys. Rev. Lett. **105**, 062301 (2010).

[13] A. Adare *et al.* (PHENIX Collaboration), Measurements of Higher-Order Flow Harmonics in Au+Au Collisions at $\sqrt{s_{NN}} = 200$ GeV, Phys. Rev. Lett. **107**, 252301 (2011).

[14] K. Aamodt *et al.* (ALICE Collaboration), Higher Harmonic Anisotropic Flow Measurements of Charged Particles in Pb-Pb Collisions at $\sqrt{s_{NN}} = 2.76$ TeV, Phys. Rev. Lett. **107**, 032301 (2011).

[15] G. Aad *et al.* (ATLAS Collaboration), Measurement of the azimuthal anisotropy for charged particle production in $\sqrt{s_{NN}} = 2.76$ TeV lead-lead collisions with the ATLAS detector, Phys. Rev. C **86**, 014907 (2012).

[16] S. Chatrchyan *et al.* (CMS Collaboration), Centrality dependence of dihadron correlations and azimuthal anisotropy harmonics in PbPb collisions at $\sqrt{s_{NN}} = 2.76$ TeV, Eur. Phys. J. C **72**, 2012 (2012).

[17] L. Adamczyk *et al.* (STAR Collaboration), Third Harmonic Flow of Charged Particles in Au+Au Collisions at $\sqrt{s_{NN}} = 200$ GeV, Phys. Rev. C **88**, 014904 (2013).

[18] B. Alver and G. Roland, Collision geometry fluctuations and triangular flow in heavy-ion collisions, Phys. Rev. C **81**, 054905 (2010); **82**, 039903(E) (2010).

[19] R. A. Lacey, A. Taranenko, N. N. Ajitanand, and J. M. Alexander, Scaling of the higher-order flow harmonics: implications for initial-eccentricity models and the 'viscous horizon', arXiv:1105.3782.

[20] F. G. Gardim, F. Grassi, M. Luzum, and J.-Y. Ollitrault, Anisotropic Flow in Event-by-Event Ideal Hydrodynamic Simulations of $\sqrt{s_{NN}} = 200$ GeV Au+Au collisions, Phys. Rev. Lett. **109**, 202302 (2012).

[21] V. Greco, C. M. Ko, and P. Levai, Parton Coalescence and Anti-Proton/Pion Anomaly at RHIC, Phys. Rev. Lett. **90**, 202302 (2003).

[22] R. J. Fries, B. Müller, C. Nonaka, and S. A. Bass, Hadronization in Heavy Ion Collisions: Recombination and Fragmentation of Partons, Phys. Rev. Lett. **90**, 202303 (2003).

[23] D. Molnar and S. A. Voloshin, Elliptic Flow at Large Transverse Momenta from Quark Coalescence, Phys. Rev. Lett. **91**, 092301 (2003).

[24] A. Adare *et al.* (PHENIX Collaboration), Scaling Properties of Azimuthal Anisotropy in Au+Au and Cu+Cu Collisions at $\sqrt{s_{NN}} = 200$ GeV, Phys. Rev. Lett. **98**, 162301 (2007).

[25] A. Adare *et al.* (PHENIX Collaboration), Systematic study of azimuthal anisotropy in Cu + Cu and Au + Au Collisions at $\sqrt{s_{NN}} = 62.4$ and 200 GeV, Phys. Rev. C **92**, 034913 (2015).

[26] L. X. Han, G. L. Ma, Y. G. Ma, X. Z. Cai, J. H. Chen, S. Zhang, and C. Zhong, Initial fluctuation effect on harmonic flow in high-energy heavy-ion collisions, Phys. Rev. C **84**, 064907 (2011).

[27] E. Schnedermann, J. Sollfrank, and U. W. Heinz, Thermal phenomenology of hadrons from 200 A/GeV S+S collisions, Phys. Rev. C **48**, 2462 (1993).

[28] P. Huovinen, P. F. Kolb, Ulrich W. Heinz, P. V. Ruuskanen, and S. A. Voloshin, Radial and Elliptic Flow at RHIC: Further Predictions, Phys. Lett. B **503**, 58 (2001).

[29] C. Adler *et al.* (STAR Collaboration), Identified Particle Elliptic Flow in Au+Au Collisions at $\sqrt{s_{NN}} = 130$ GeV, Phys. Rev. Lett. **87**, 182301 (2001).

[30] H Masui, Ph.D. thesis, Tsukuba University, 2007.

[31] K. Adcox *et al.* (PHENIX Collaboration), Phenix detector overview, Nucl. Instrum. Methods Phys. Res., Sec. A **499**, 469 (2003).

[32] K. Adcox *et al.* (PHENIX Collaboration), PHENIX central arm tracking detectors, Nucl. Instrum. Methods Phys. Res., Sec. A **499**, 489 (2003).

[33] A. Adare *et al.* (PHENIX Collaboration), Deviation from quark-number scaling of the anisotropy parameter v_2 of pions, kaons, and protons in Au+Au collisions at $\sqrt{s_{NN}} = 200$ GeV, Phys. Rev. C **85**, 064914 (2012).

[34] E. Richardson *et al.* (PHENIX Collaboration), A Reaction Plane Detector for PHENIX at RHIC, Nucl. Instrum. Methods Phys. Res., Sec. A **636**, 99 (2011).

[35] S. Afanasiev *et al.* (PHENIX Collaboration), Systematic Studies of Elliptic Flow Measurements in Au+Au Collisions at $\sqrt{s} =$ 200 GeV, Phys. Rev. C **80**, 024909 (2009).

[36] T. Todoroki and T. Niida, doctoral theses, University of Tsukuba, 2014 [http://www.phenix.bnl.gov/WWW/talk/theses.php].

[37] R. A. Lacey (PHENIX Collaboration), Elliptic flow measurements with the PHENIX detector, Nucl. Phys. A **698**, 559 (2002).

[38] K. Adcox *et al.* (PHENIX Collaboration), Flow measurements via two particle azimuthal correlations in Au+Au collisions at $\sqrt{s_{NN}} = 130$ GeV, Phys. Rev. Lett. **89**, 212301 (2002).

[39] H. Masui and A. Schmah, Event plane resolution correction for azimuthal anisotropy in wide centrality bins, arXiv:1212.3650.

[40] G. Aad *et al.* (ATLAS Collaboration), Measurement of event-plane correlations in $\sqrt{s_{NN}} = 2.76$ TeV lead-lead collisions with the ATLAS detector, Phys. Rev. C **90**, 024905 (2014).

[41] L. Yan and J.-Y. Ollitrault, v_4, v_5, v_6, v_7: Nonlinear hydrodynamic response versus LHC data, Phys. Lett. B **744**, 82 (2015).

[42] P. F. Kolb, L.-W. Chen, V. Greco, and C. M. Ko, Momentum anisotropies in the quark coalescence model, Phys. Rev. C **69**, 051901 (2004).

[43] M. Luzum, C. Gombeaud, and J.-Y. Ollitrault, v_4 in ideal and viscous hydrodynamics simulations of nuclear collisions at the BNL Relativistic Heavy Ion Collider (RHIC) and the CERN Large Hadron Collider (LHC), Phys. Rev. C **81**, 054910 (2010).

[44] N. Borghini and J.-Y. Ollitrault, Momentum spectra, anisotropic flow, and ideal fluids, Phys. Lett. B **642**, 227 (2006).

[45] C.-J. Zhang and J. Xu, Investigating the scaling of higher-order flows in relativistic heavy-ion collisions, Phys. Rev. C **93**, 024906 (2016).

[46] S. S. Adler *et al.* (PHENIX Collaboration), Identified charged particle spectra and yields in Au+Au collisions at $\sqrt{s_{NN}} = 200$ GeV, Phys. Rev. C **69**, 034909 (2004).

[47] S. S. Adler *et al.* (PHENIX Collaboration), Production of phi mesons at mid-rapidity in $\sqrt{s_{NN}} = 200$ GeV Au+Au collisions at RHIC, Phys. Rev. C **72**, 014903 (2005).

[48] M. L. Miller, K. Reygers, S. J. Sanders, and P. Steinberg, Glauber modeling in high energy nuclear collisions, Ann. Rev. Nucl. Part. Sci. **57**, 205 (2007).

[49] A. Adare *et al.* (PHENIX Collaboration), Azimuthal-Angle Dependence of Charged-Pion-Interferometry Measurements with Respect to Second- and Third-Order Event Planes in Au + Au Collisions at $\sqrt{s_{NN}} = 200$ GeV, Phys. Rev. Lett. **112**, 222301 (2014).